PCCP

Physical Chemistry Chemical Physics

This paper is published as part of a PCCP Themed Issue on:

Interfacial Systems Chemistry: Out of the Vacuum, Through the Liquid, Into the Cell

Guest Editors: Professor Armin Gölzhäuser (Bielefeld) & Professor Christof Wöll (Karlsruhe)

Editorial

Interfacial systems chemistry: out of the vacuum—through the liquid—into the cell
Phys. Chem. Chem. Phys., 2010
DOI: 10.1039/c004746p

Perspective

The role of "inert" surface chemistry in marine biofouling prevention
Axel Rosenhahn, Sören Schilp, Hans Jürgen Kreuzer and Michael Grunze, *Phys. Chem. Chem. Phys.*, 2010
DOI: 10.1039/c001968m

Communication

Self-assembled monolayers of polar molecules on Au(111) surfaces: distributing the dipoles
David A. Egger, Ferdinand Rissner, Gerold M. Rangger, Oliver T. Hofmann, Lukas Wittwer, Georg Heimel and Egbert Zojer, *Phys. Chem. Chem. Phys.*, 2010
DOI: 10.1039/b924238b

Is there a Au–S bond dipole in self-assembled monolayers on gold?
LinJun Wang, Gerold M. Rangger, ZhongYun Ma, QiKai Li, Zhigang Shuai, Egbert Zojer and Georg Heimel, *Phys. Chem. Chem. Phys.*, 2010
DOI: 10.1039/b924306m

Papers

Heterogeneous films of ordered CeO_2/Ni concentric nanostructures for fuel cell applications
Chunjuan Zhang, Jessica Grandner, Ran Liu, Sang Bok Lee and Bryan W. Eichhorn, *Phys. Chem. Chem. Phys.*, 2010
DOI: 10.1039/b918587a

Synthesis and characterization of RuO_2/poly(3,4-ethylenedioxythiophene) composite nanotubes for supercapacitors
Ran Liu, Jonathon Duay, Timothy Lane and Sang Bok Lee, *Phys. Chem. Chem. Phys.*, 2010
DOI: 10.1039/b918589p

Bending of purple membranes in dependence on the pH analyzed by AFM and single molecule force spectroscopy
R.-P. Baumann, M. Schranz and N. Hampp, *Phys. Chem. Chem. Phys.*, 2010
DOI: 10.1039/b919729j

Bifunctional polyacrylamide based polymers for the specific binding of hexahistidine tagged proteins on gold surfaces
Lucas B. Thompson, Nathan H. Mack and Ralph G. Nuzzo, *Phys. Chem. Chem. Phys.*, 2010
DOI: 10.1039/b920713a

Self-assembly of triazatriangulenium-based functional adlayers on Au(111) surfaces
Sonja Kuhn, Belinda Baisch, Ulrich Jung, Torben Johannsen, Jens Kubitschke, Rainer Herges and Olaf Magnussen, *Phys. Chem. Chem. Phys.*, 2010
DOI: 10.1039/b922882a

Polymer confinement effects in aligned carbon nanotubes arrays
Pitamber Mahanandia, Jörg J. Schneider, Marina Khaneft, Bernd Stühn, Tiago P. Peixoto and Barbara Drossel, *Phys. Chem. Chem. Phys.*, 2010
DOI: 10.1039/b922906j

Single-stranded DNA adsorption on chiral molecule coated Au surface: a molecular dynamics study
Haiqing Liang, Zhenyu Li and Jinlong Yang, *Phys. Chem. Chem. Phys.*, 2010
DOI: 10.1039/b923012b

Protein adsorption onto CF_3-terminated oligo(ethylene glycol) containing self-assembled monolayers (SAMs): the influence of ionic strength and electrostatic forces
Nelly Bonnet, David O'Hagan and Georg Hähner, *Phys. Chem. Chem. Phys.*, 2010
DOI: 10.1039/b923065n

Relative stability of thiol and selenol based SAMs on Au(111) — exchange experiments
Katarzyna Szelągowska-Kunstman, Piotr Cyganik, Bjorn Schüpbach and Andreas Terfort, *Phys. Chem. Chem. Phys.*, 2010
DOI: 10.1039/b923274p

Micron-sized [6,6]-phenyl C61 butyric acid methyl ester crystals grown by dip coating in solvent vapour atmosphere: interfaces for organic photovoltaics
R. Dabirian, X. Feng, L. Ortolani, A. Liscio, V. Morandi, K. Müllen, P. Samorì and V. Palermo, *Phys. Chem. Chem. Phys.*, 2010
DOI: 10.1039/b923496a

Self-assembly of L-glutamate based aromatic dendrons through the air/water interface: morphology, photodimerization and supramolecular chirality
Pengfei Duan and Minghua Liu, *Phys. Chem. Chem. Phys.*, 2010
DOI: 10.1039/b923595g

Self-assembled monolayers of benzylmercaptan and *para*-cyanobenzylmercaptan on gold: surface infrared spectroscopic characterization
K. Rajalingam, L. Hallmann, T. Strunskus, A. Bashir, C. Wöll and F. Tuczek, *Phys. Chem. Chem. Phys.*, 2010
DOI: 10.1039/b923628g

The formation of nitrogen-containing functional groups on carbon nanotube surfaces: a quantitative XPS and TPD study
Shankhamala Kundu, Wei Xia, Wilma Busser, Michael Becker, Diedrich A. Schmidt, Martina Havenith and Martin Muhler, *Phys. Chem. Chem. Phys.*, 2010
DOI: 10.1039/b923651a

Geometric and electronic structure of Pd/4-aminothiophenol/Au(111) metal–molecule–metal contacts: a periodic DFT study
Jan Kučera and Axel Groß, *Phys. Chem. Chem. Phys.*, 2010
DOI: 10.1039/b923700c

Ultrathin conductive carbon nanomembranes as support films for structural analysis of biological specimens
Daniel Rhinow, Janet Vonck, Michael Schranz, Andre Beyer, Armin Gölzhäuser and Norbert Hampp, *Phys. Chem. Chem. Phys.*, 2010
DOI: 10.1039/b923756a

Microstructured poly(2-oxazoline) bottle-brush brushes on nanocrystalline diamond
Naima A. Hutter, Andreas Reitinger, Ning Zhang, Marin Steenackers, Oliver A. Williams, Jose A. Garrido and Rainer Jordan, *Phys. Chem. Chem. Phys.*, 2010
DOI: 10.1039/b923789p

Model non-equilibrium molecular dynamics simulations of heat transfer from a hot gold surface to an alkylthiolate self-assembled monolayer
Yue Zhang, George L. Barnes, Tianying Yan and William L. Hase, *Phys. Chem. Chem. Phys.*, 2010
DOI: 10.1039/b923858c

Holey nanosheets by patterning with UV/ozone
Christoph T. Nottbohm, Sebastian Wiegmann, André Beyer and Armin Gölzhäuser, *Phys. Chem. Chem. Phys.*, 2010
DOI: 10.1039/b923863h

Tuning the local frictional and electrostatic responses of nanostructured $SrTiO_3$—surfaces by self-assembled molecular monolayers
Markos Paradinas, Luis Garzón, Florencio Sánchez, Romain Bachelet, David B. Amabilino, Josep Fontcuberta and Carmen Ocal, *Phys. Chem. Chem. Phys.*, 2010
DOI: 10.1039/b924227a

Influence of OH groups on charge transport across organic–organic interfaces: a systematic approach employing an "ideal" device
Zhi-Hong Wang, Daniel Käfer, Asif Bashir, Jan Götzen, Alexander Birkner, Gregor Witte and Christof Wöll, *Phys. Chem. Chem. Phys.*, 2010
DOI: 10.1039/b924230a

A combinatorial approach toward fabrication of surface-adsorbed metal nanoparticles for investigation of an enzyme reaction
H. Takei and T. Yamaguchi, *Phys. Chem. Chem. Phys.*, 2010
DOI: 10.1039/b924233n

Structural characterization of self-assembled monolayers of pyridine-terminated thiolates on gold
Jinxuan Liu, Björn Schüpbach, Asif Bashir, Osama Shekhah, Alexei Nefedov, Martin Kind, Andreas Terfort and Christof Wöll, *Phys. Chem. Chem. Phys.*, 2010
DOI: 10.1039/b924246p

Quantification of the adhesion strength of fibroblast cells on ethylene glycol terminated self-assembled monolayers by a microfluidic shear force assay
Christof Christophis, Michael Grunze and Axel Rosenhahn, *Phys. Chem. Chem. Phys.*, 2010
DOI: 10.1039/b924304f

Lipid coated mesoporous silica nanoparticles as photosensitive drug carriers
Yang Yang, Weixing Song, Anhe Wang, Pengli Zhu, Jinbo Fei and Junbai Li, *Phys. Chem. Chem. Phys.*, 2010
DOI: 10.1039/b924370d

On the electronic and geometrical structure of the *trans*- and *cis*-isomer of tetra-*tert*-butyl-azobenzene on Au(111)
Roland Schmidt, Sebastian Hagen, Daniel Brete, Robert Carley, Cornelius Gahl, Jadranka Dokić, Peter Saalfrank, Stefan Hecht, Petra Tegeder and Martin Weinelt, *Phys. Chem. Chem. Phys.*, 2010
DOI: 10.1039/b924409c

Oriented growth of the functionalized metal–organic framework CAU-1 on –OH- and –COOH-terminated self-assembled monolayers
Florian Hinterholzinger, Camilla Scherb, Tim Ahnfeldt, Norbert Stock and Thomas Bein, *Phys. Chem. Chem. Phys.*, 2010
DOI: 10.1039/b924657f

Interfacial coordination interactions studied on cobalt octaethylporphyrin and cobalt tetraphenylporphyrin monolayers on Au(111)
Yun Bai, Michael Sekita, Martin Schmid, Thomas Bischof, Hans-Peter Steinrück and J. Michael Gottfried, *Phys. Chem. Chem. Phys.*, 2010
DOI: 10.1039/b924974p

Probing adsorption and aggregation of insulin at a poly(acrylic acid) brush
Florian Evers, Christian Reichhart, Roland Steitz, Metin Tolan and Claus Czeslik, *Phys. Chem. Chem. Phys.*, 2010
DOI: 10.1039/b925134k

Nanocomposite microstructures with tunable mechanical and chemical properties
Sameh Tawfick, Xiaopei Deng, A. John Hart and Joerg Lahann, *Phys. Chem. Chem. Phys.*, 2010
DOI: 10.1039/c000304m

A combinatorial approach toward fabrication of surface-adsorbed metal nanoparticles for investigation of an enzyme reaction†

H. Takei* and T. Yamaguchi

Received 17th November 2009, Accepted 12th February 2010
First published as an Advance Article on the web 25th March 2010
DOI: 10.1039/b924233n

We are presenting a combinatorial approach for the preparation of surface-adsorbed metal nanoparticles for investigation of biological phenomena. Metal nanoparticles, in particular noble metal nanoparticles, have become increasingly recognized for their importance in studies of biological systems. An intense near-field associated with these particles can be exploited to improve the performance of various spectroscopic techniques. In this paper, we combine the metal nanoparticle with a colorimetric enzyme reaction and explore spectral changes of the metal nanoparticle dependent on the extent of the reaction, alkaline phosphatase acting on nitro-blue tetrazolium chloride. Changing the shape of the gold particle has a clear effect on the extent of the spectral shift. Furthermore, we demonstrate that the method we employ for preparation of metal particles, vacuum evaporation of a metal on a monolayer of surface-adsorbed monodisperse polystyrene or silica nanospheres, is supremely suited for a combinatorial approach. By depositing two different metals on nanospheres as multi-layers while varying the ratio as well as absolute thicknesses, it is possible to produce a large variety of metal particles in parallel. We show the potential of such a combinatorial approach for rapidly producing metal nanoparticles of choice.

Introduction

In recent years, metal nanoparticles have been receiving ever increasing attention in wide-ranging fields associated with biological sciences.[1–7] New uses have been found for existing gold colloids while more complex nanoparticles have also become available.[8–13] For one, researchers have begun to pay attention to control of free electrons in noble metal nanoparticles. For example, change in color of gold colloids upon aggregation has been exploited for exquisite detection of DNA hybridization. Mirkin *et al.* showed that a mismatched hybridization can be detected *via* observation of the melting curve.[14] They used as a detection technique the change in color of gold colloids upon aggregation due to hybridization. Surface-adsorbed gold nanoparticles have also become the target of intense research.[15–21] One application is non-labeled real-time detection of biological binding events. When the gold nanoparticle is first modified with an antibody or receptor molecule and the corresponding antigen or ligand binds to the surface due to a specific binding, the color of gold nanoparticles changes because the local refractive index is different after the binding event. As has been known for a number of years, the resonance peak wavelength depends exquisitely on the surrounding refractive index.[22–27]

It has become possible to prepare gold particles other than spheres[28,29] and they all show interesting optical properties. When a gold nano-shell is formed around a non-metallic core, the peak absorbance was found to shift toward longer wavelength. Particles absorbing in near-infrared have intriguing applications, and the field of metal nanoshells has been rapidly expanding.[3] The rod is another shape that has been explored widely recently.[30,31]

While these particles can be applied in various ways, Raman spectroscopy is one spectroscopic technique that has benefited from new developments because intrinsically weak Raman signals can be enhanced over million fold if the target molecule is placed in the vicinity of appropriate noble metal nanostructures.[11,32–36] The intense near-field is thought to contribute significantly to the signal enhancement. Surface-enhanced infrared spectroscopy has also been studied.[37–39] Fluorescence spectroscopy is another technique that has become associated with noble metal nanoparticles, in particular silver.[40–45] With a sandwiched immunoassay, it has been shown that it is possible to obtain quantitative data, critical for many clinical applications.[46–49]

In this paper, we will show preliminary data indicating the potential of noble metal nanoparticles for enhancing the sensitivity of colorimetric enzyme assays. They are popular as rapid and simple clinical diagnostic tools.[2] With a sandwich immunoassay, the secondary antibody is modified with an enzyme such as alkaline phosphatase, ALP, or horseradish peroxidase, HRP. The reaction with an appropriate substrate results in formation of a colorful insoluble product, allowing reading of the result with the naked eye. When the enzyme reaction is carried out over gold nanoparticles, however, the deposition of the insoluble product leads to a change in the absorption spectrum. The detection is thus carried out not directly by the appearance of the colorful product but indirectly from the spectral shift of the underlying gold particles.

Faculty of Life Sciences, Toyo University, Itakura, Gunma 374-0193, Japan
† Electronic supplementary information (ESI) available: Figures S1 and S2. See DOI: 10.1039/b924233n

A control experiment was carried out to show that the appearance of the reaction product can be detected more sensitively over the gold nanoparticle surface than a plane gold surface. The insoluble product absorbs below 650 nm so that its presence can be detected directly, but our method of detecting the refractive index change *via* localized surface plasmon promises to improve the detection limit. Furthermore, we will attempt to correlate the change in the spectrum with the amount of the product deposited on gold particles.

Our method of forming metal nanoparticle, deposition of a metal onto a monolayer of monodisperse polystyrene or silica nanospheres on a flat surface allows us to readily manipulate the optical properties. Of two parameters under control, deposition thickness and sphere diameter, we report in the work the effect of modifying the deposition thickness. While almost all samples produced exhibit some absorption peak, the change the absorption spectrum undergoes upon enzyme reaction depends significantly on the metal deposition thickness. It will be shown that optimization is rather straightforward.

Finally, we will give a glimpse of the power of this technique for forming a variety of metal nanoparticles. The metal deposition is obviously not limited to a single species; multiple metal layers can be deposited. As one example, we will show properties of metal nanoparticles consisting of gold and silver. Mixing of metals has been explored,[50–53] and we have found that our investigation can benefit from such a procedure. We will show that the peak shift due to deposition of ALP-induced product can be enhanced. A combinatorial approach for metal nanoparticle production is likely to have further implications.[54]

Experimental

The materials were purchased as follows: surfactant-free polystyrene nanospheres and silica microspheres were from JSR Corp. (Tokyo, Japan) and Polysciences, Inc. (Warrington, PA, USA) respectively. Alkaline phosphatase, ALP, was purchased from Wako (Nippon Gene, Cat. No. 319-02661) and diluted in Tris buffered saline (TBS) purchased from Polysciences (Cat. No. 24082). Nitro-blue tetrazolium chloride 5-bromo-4-chloro-3′-indolylphosphatase *p*-toluidine salt, NBT/BCIP, was purchased from Pierce. Gold (99.99% purity) was purchased from Tanaka Kikinzoku Kogyo, K.K. Both silver (99.999% purity) and copper (99.99% purity) were purchased from Kohjyundo Kagaku K.K.

Sphere adsorption

The crucial step in our method is preparation of a uniformly adsorbed nanosphere monolayer. While the process is described in detail elsewhere, we give a brief description here. Nanopheres suspended in a solution are prevented from aggregation by a repulsive force. We have found that careful and well-controlled reduction of the repulsive force in the presence of a high energy surface leads to formation of a sphere monolayer; both polystyrene and silica spheres being used. As a high-energy surface, glass slides (Micro Slide Glass, S2442, Matsunami Glass, Ltd.) without further cleaning were coated by 20 nm of gold by thermal evaporation as described below. It is crucial that a residual repulsive force remains; otherwise spheres would build up, leading to formation of a multilayer. For the purpose of making uniform particles, it is imperative that a monolayer be formed. For the reduction of the repulsive force, we have found that a water-soluble carbodiimide (1-ethyl 3-(3-(dimethylamino) propyl) carbodiimide, EDC) serves a useful purpose.

Metal evaporation

Metal evaporation was carried out within an evaporator from Ulvac Kohki (Tokyo, Japan), DEPOX VFR-200M/ERH, at the base pressure of 5×10^{-3} Pa with a typical deposition rate of 0.1 nm per second.

Optical detection

Reflectance spectra of the samples were obtained with Ocean Optics USB4000 equipped with a custom-made quartz fibre bundle (Tsuchida, Tokyo, Japan) consisting of a single 100 μm fibre, surrounded by six other fibres of the same diameter. The surrounding fibres were used for illumination of the sample with light from a tungsten halogen lamp (LS-1-LL), and the central fibre is for detection of reflected light from the sample. As for reference, a glass slide coated with an equivalent amount of metal was used. For example, for characterization of silver particles prepared by depositing 10 nm of silver on silica particles adsorbed on a 20 nm thick gold film underneath, the reference sample would have a 20 nm thick gold and 10 nm thick silver on the glass slide.

Alkaline phosphotase reaction

For this reaction, a well was formed around each particle spot by placing a silicone gasket with 3 mm diameter holes (CultureWell, Cat. No. C-24780, Invitrogen). Five μl of the diluted solution were added to a single spot. After 5 min incubation, the spot was rinsed with TBS three times. The optical fibre described in Optical Detection Section was placed over the spot, and 10 μl of TBS was added to fill the well. A custom-made software from Tamon Inc. was used that can capture spectra sequentially at a pre-determined time interval. Within a few seconds after the spectrum capture sequence was initiated, 5 μl of NBT/BCIP was added to the well to start the enzyme reaction. The optical fibre was equipped with a miniature mixing mechanism insuring constant agitation of the solution during observation.

Electron microscopy

Samples were observed with a scanning electron microscope (JSM 7400 F, JEOL, Tokyo, Japan).

Results

Fig. 1(a) is a schematic diagram showing the preparation protocol of metal nanoparticles. A substrate covered by a monolayer of monodisperse nanospheres is the starting point. The detailed protocol is described elsewhere,[48,55] but a short summary is given here; nanospheres suspended in an aqueous solution are induced partially to aggregate by judicious increase in the salt concentration. Exposure of a high energy surface to the solution leads rapidly to formation of a sphere

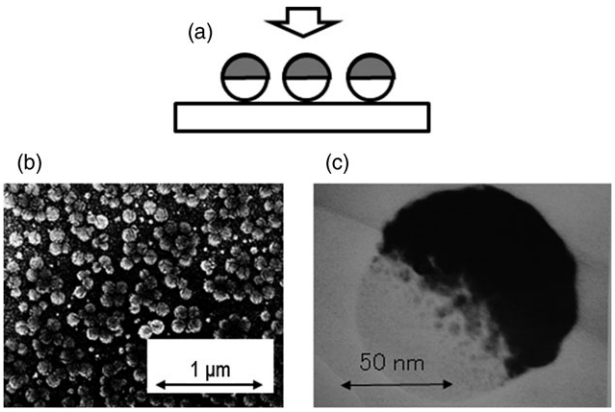

Fig. 1 Schematic diagram for metal nanoparticle preparation and a photo of the resulting nanoparticles. Section (a) shows the method with which hemispherical metal nanoparticles are formed: firstly, a dense monolayer of monodisperse polystyrene or silica nanospheres is formed on a glass substrate coated with a gold film, 20 nm thick. Secondly, a metal of choice is evaporated on top of the nanosphere monolayer. Photo (b) is a scanning electron micrograph of the resulting sample, and photo (c) is a transmission electron micrograph of one sphere dislodged from the substrate.

monolayer on the surface; the adsorption process is mostly complete within the first ten seconds, but the process is allowed to proceed for five minutes or longer to assure the uniformity of the sample quality. Fig. 1(b) is an SEM micrograph of gold nanoparticles. Spheres are adsorbed in a dense and random fashion. Most nanoparticles exist in contact with neighboring nanoparticles, forming clusters. Fig. 1(c) is a transmission electron microscope (TEM) micrograph of a dislodged sphere (courtesy of Dr T. Matsumoto of Hitachi Ltd.). The dark region is the metal, and the light region is the nanosphere. The hemispherical shape is typical, and almost all particles exhibit the same morphology. The fact that we use a nanosphere monolayer is important because with an additional layer, the top layer would function as a mask so that metal nanoparticles formed on the top and lower layers would not share the same morphology.

Fig. 2(a) are spectra of gold nanoparticles obtained by depositing gold with different thicknesses. As the deposition thickness is increased from 10 to 25 nm, the peak found around 690 nm for 10 nm deposition grows in intensity while shifting toward longer wavelengths. The current spectrometer does not have sufficient sensitivity beyond 900 nm so that the spectra in Fig. 2 are somewhat distorted, but a near-IR spectrometer on short loan with the range up to 1400 nm revealed that the peak does not disappear as seems with thicker deposition thicknesses, but rather it shifts smoothly toward longer wavelengths (not shown). At the same time, the shoulder originally observed around 500 nm grows gradually into a peak, with the peak wavelength around 530 nm. In interpreting these peaks, the presence of the underlying gold layer cannot be ignored. It was shown that the underlying gold layer enhanced the peak intensity,[27,48] and a more systematic study by Tamiya *et al*. has confirmed the initial observation.[56] While not shown here, the growth of the 500 nm shoulder is significantly more pronounced in the presence of the

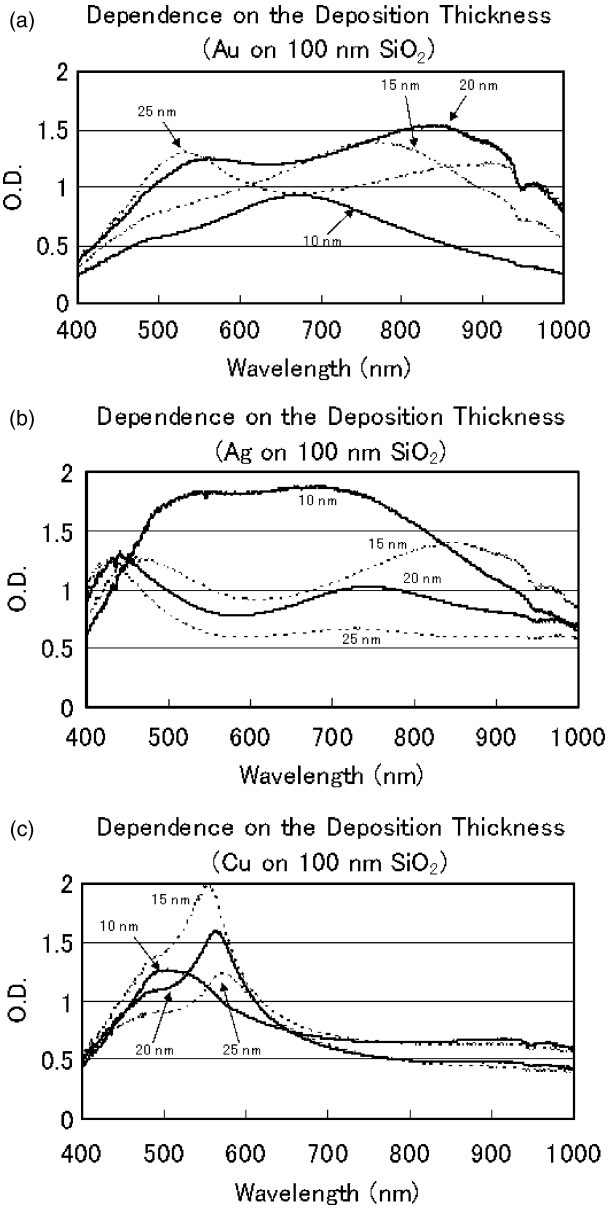

Fig. 2 Absorption spectra of various metal nanoparticles. Gold (a), silver (b) and copper (c) were evaporated on 100 nm silica nanospheres with varying deposition thicknesses, 10, 15, 20, and 25 nm.

underlying gold layer, the 670 nm peak is still observed in the absence of the underlying layer, albeit at 725 nm. This suggests that the peak at the shorter wavelength reflect more of a cavity property, the one formed by the top and bottom gold layers.

Fig. 2(b) and (c) are, respectively, for silver and copper, similar to gold in Fig. 2(a). The silver nanoparticle is characterized by the broad and intense absorbance when formed by 10 nm deposition and the growth of a peak below 450 nm. As for copper, relatively sharper peaks appear in a narrower wavelength region. The peak shifts toward the longer wavelengths with the increase in the deposition thickness. Within the deposition thickness range explored in this paper, the peak intensity diminished as the deposition thickness increased. Fig. 3 contains photos of the metal

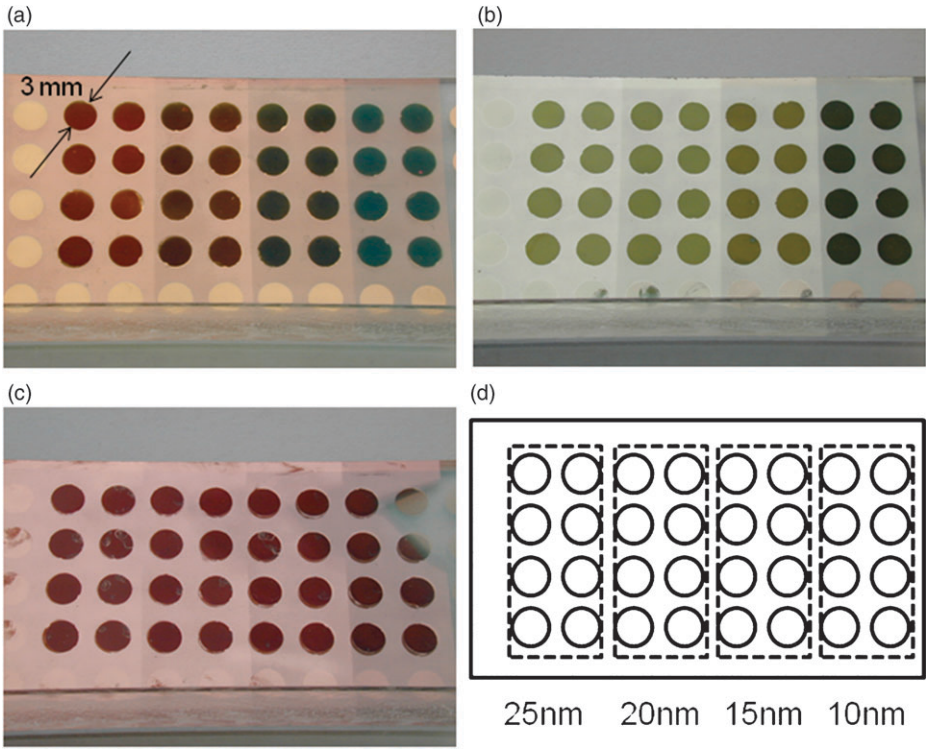

Fig. 3 Photos of gold (a), silver (b) and copper (c) samples used to obtain spectra in Fig. 2. In each photo, eight columns are grouped into four, each with eight identical spots, of different deposition thicknesses. From left to right, the deposition thickness is 25, 20, 15, and 10 nm.

nanoparticle samples whose spectra are shown in Fig. 2. The spot diameter is 3 mm. The quality uniformity can be confirmed.

We show how an enzyme reaction induces changes in the absorption peak. For this experiment, we used predominantly gold due to its stability in a buffer solution. The ALP molecule physisorbs well onto gold surfaces. Addition of the NBT/BCIP substrate leads to formation of an insoluble product. It is possible to control the amount of the product by adjusting the amount of ALP on gold surfaces, or controlling the reaction time. Initially we adsorbed large amounts of ALP, close to the saturation limit, and observed the general trend in the peak shift. Fig. 4 shows a series of spectra for gold nanoparticles formed by deposition of 25, 20, 15, and 10 nm of gold, corresponding to (a), (b), (c) and (d). Note that the peak intensity and the peak wavelength are different from Fig. 2 because here the spectra were obtained while submerged in the TBS buffer. For example, with 25 nm deposition, the peak wavelength is at 530 and 550 nm, respectively, when the sample is in the air or submerged in the buffer. The dependence of the peak wavelength on the refractive index of the surrounding environment has been reported, [22] and the shifted peak in Fig. 4 simply reflects this. For (a), (b) and (d), the peak increases in intensity and exhibits red shifts. The fifteen nanometer deposition stands out because there are two distinct peaks, one being a shoulder before formation of the insoluble. The broad peak around 805 nm red-shifts rapidly as the shoulder around 650 nm grows into a peak. As mentioned earlier, the lack of sensitivity in the current spectrometer above 900 nm does not reveal the structure, but the peak does not disappear; rather it shifts smoothly beyond 1000 nm. Difference spectra, corresponding to the change before and after the enzyme reaction, are shown in Fig. 5

To see whether the use of such a particle surface really has an advantage in development of a colorimetric detection device, we carried out an identical reaction on a plane gold surface as shown in Fig. 6. The insoluble product of the ALP reaction absorbs over a wide visible region, particularly in the blue. Simply monitoring the change in absorption allows one to track the formation of the product. With the same protocol, the change in optical density is less than 0.2 around 475 nm, which contrasts with 0.7 or so with the aid of gold nanoparticles as is seen in Fig. 5. Simple comparison in terms of the optical density change does not do justice, however. From the analytical perspective, monitoring of the peak shift is a more reliable indicator than change in absorbance.

We carried out further comparisons by lowering the ALP concentration. Spectra shown in Fig. 7 are spectra obtained from the control experiment, *i.e.*, the enzyme reaction on a plane gold surface, when ALP solutions of different concentrations were used for physisoption. The reaction time was two minutes. The dilution of the ALP solution 5000 fold pushed it to the detection limit. The absorption below 450 nm is due to the NBT/BCIP solution itself rather than that of the insoluble product.

In contrast, Fig. 8 shows how the spectrum of gold nanoparticles (15 nm gold deposition) shifts with ALP diluted 5000 fold. These spectra reflect a two-minute progress. In terms of change in optical density, the change of 0.3 is greater than 0.18 as obtained with the control experiment with ALP diluted 200 fold.

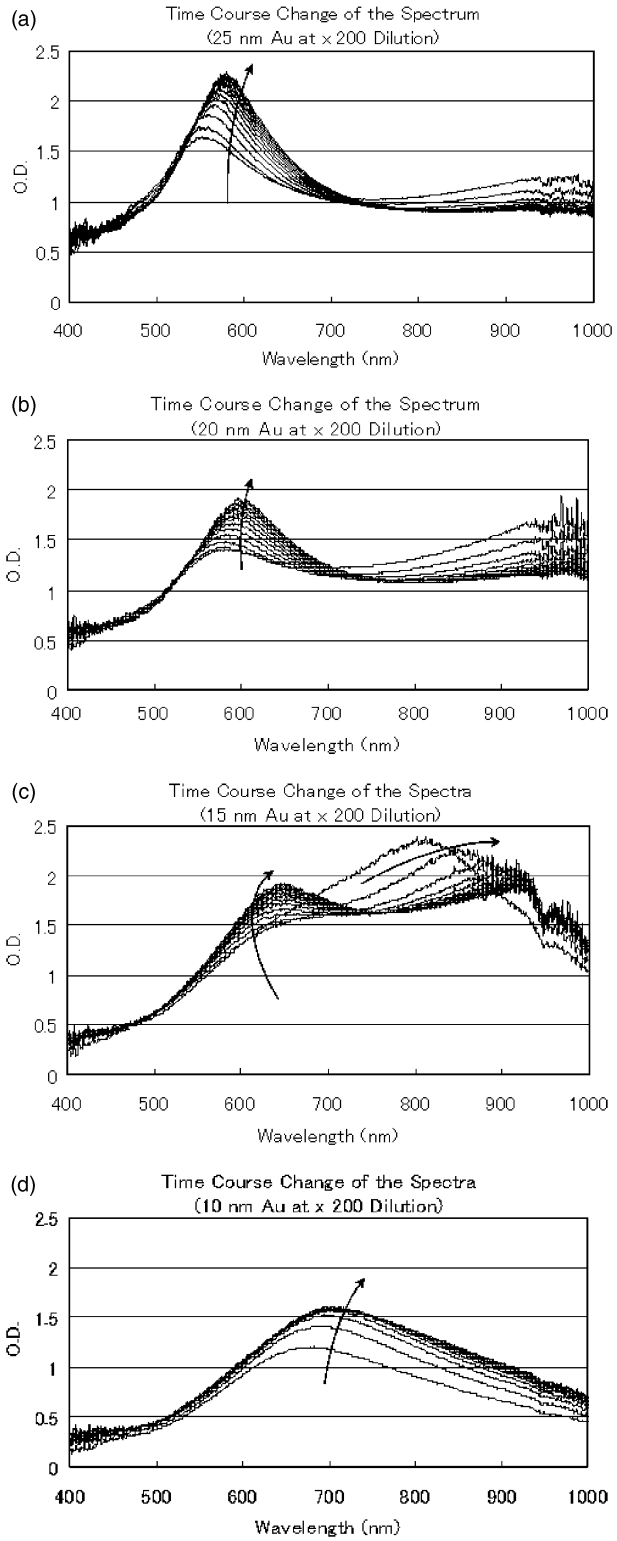

Fig. 4 Shift in the peak induced by the enzyme reaction. Results are shown for gold nanoparticles with 25, 20, 25, and 10 nm of deposition. Alkaline phosphatase, ALP, physisorbed on gold nanoparticles were made to react with the substrate, NBT/BCIP. The insoluble product of the reaction adhered to the gold particle. Gold particles were exposed to 6 μl of the diluted ALP solution for 15 min at room temperature. After rinsing of gold particles with TBS, 10 μl of the substrate, NBT/BCIP, was injected into the well within a few seconds after recording was initiated. Spectra were obtained sequentially every 10 s for 2 min.

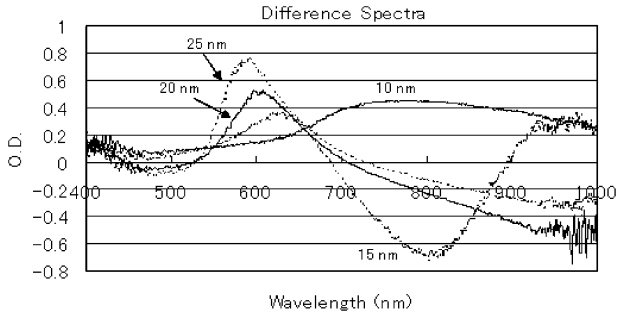

Fig. 5 Difference spectra of gold nanoparticles before and after the ALP reaction.

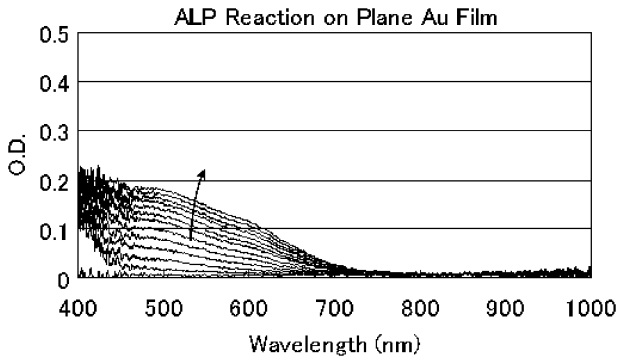

Fig. 6 The ALP reaction on gold surface. A plane gold surface, 20 nm thick, was used as the surface instead of gold particles. The enzyme reaction is identical to those reactions in Fig. 4. The initial absorption below 440 nm is due to the NBT/BCIP solution.

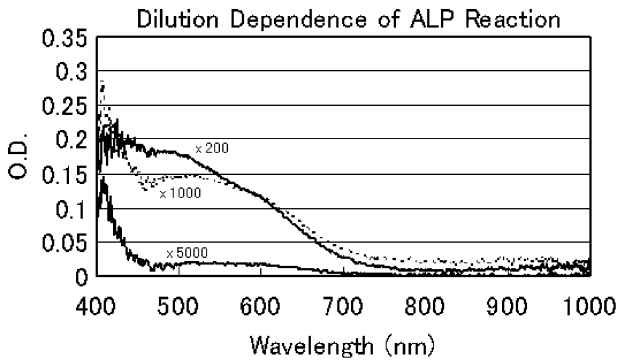

Fig. 7 ALP control experiment at different concentrations. ALP solutions diluted 200, 1000 and 5000 fold were used to attach ALP molecules onto gold particles. There was no increase in the absorption with ALP diluted 5000 fold.

The photo in Fig. 9 show color changes in gold nanoparticles after the ALP reaction. These spots are grouped in four, with deposition thicknesses of 25, 20, 15 and 10 nm from left to right. Within each group, four pairs of spots show changes induced by ALP diluted 25 000, 5000, 1000 and 200 fold. With the 25 000 dilution, there is hardly any change in appearance, but with 1000 fold dilution, there is a visible change.

To gain an insight into the sensitivity of the color change, we carried out the ALP reaction for various time durations. Then, we characterized each sample with both the optical

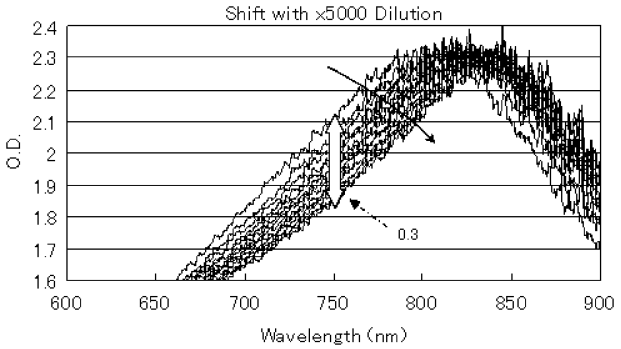

Fig. 8 Shifts in the spectrum of 15 nm gold nanoparticles with ALP diluted 5000 fold. Unlike the control experiment with a plane gold surface shown in Fig. 7, the shifts are quite noticeable, and the intensity shift is 0.3 around 750 nm.

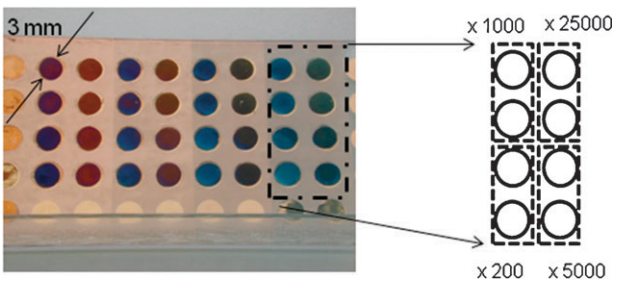

Fig. 9 A photo showing appearance changes of gold nanoparticles after the ALP reaction. As with photos in Fig. 4, eight columns are grouped into four, with 25, 20, 15 and 10 nm gold deposition from left to right. Within each group, top two spots in the right column have been exposed to ALP solution diluted 25 000 fold, and bottom two spots in the same column have been exposed to 5000 fold diluted ALP solution. For the left column, the top two and bottom two have been respectively exposed to ALP solutions diluted 1000 and 200 fold. The enzyme reaction was 2 min long for all cases. No change in color was noticed for those spots exposed to ALP solution diluted 25000 fold, being identical to the naked eye for unreacted spots.

method and SEM observation. Fifteen-nm thick gold nanoparticles were exposed to ALP diluted 1000 fold, and the enzyme reaction was allowed to proceed for 1, 3 and 5 min. Fig. 10 shows the spectra of these samples as measured in the air. SEM micrographs in Fig. 11 are obtained from the very same samples. While accurate assessment of the thickness of the deposited insoluble product is not possible, the maximum deposition thickness after 5 min reaction (Fig. 11(d)) is estimated to be less than 10 nm, using the nanosphere size as the reference. If a simple interpolation applies, the deposition thickness for Fig. 11(b) is some 2 nm. In Fig. 10, the optical density change at its maximum is 0.5, around 780 nm, after 1 min reaction.

Next, we present data with multi-layer metal nanoparticles. The photo in Fig. 12 is an array of silver/gold multilayer metal particles whereby gold was first deposited, followed by silver. Along the horizontal direction, the deposition thickness was varied from 5 to 40 nm with a 5 nm increment. Along the vertical direction, the silver deposition thickness was varied from 0 to 7.5 nm with a 2.5 nm increment. It is interesting to note that the difference in appearance between 5 nm gold

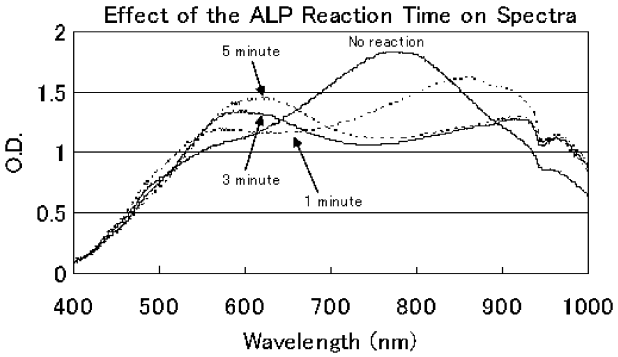

Fig. 10 Dependence of the spectrum shift upon the reaction time. Results for gold nanoparticles prepared by 15 nm deposition are shown because the change was most noticeable. Note that these spectra were obtained in the air, rather than in solutions in the earlier figures.

nanoparticles (spot 1) and 5nmAg/5nmAu particles (spot 2) is much more than that between 5 nm and 10 nm gold particles (spots 1 and 3). One can look at it as the influence on 5 nm gold particles by 5 nm silver or gold depositions. As the thickness of gold increases, additional silver deposition has a diminishing influence.

Fig. 13 contains spectra of most spots from the sample shown in Fig. 12. Some spots not shown; for thicker gold deposition thicknesses, they are quite similar to those with slightly thinner deposition thicknesses. Fig. S1 (see the ESI†) shows results of performing the ALP reaction on some of the multi-layered metal particles. Looking at Fig. S1(c), with 5 nm silver on 10 nm gold, it is clear that the spectrum clearly differs from 15 nm gold. The longer wavelength peak of the multi-layered particle does not undergo as much change as with the pure gold nanoparticle. On the other hand, the 2.5 nm silver deposition may have an overall positive effect. Changes in the peak wavelength and intensity are plotted for both 10 nm gold and 2.5 nm Ag/10 nm Au particles in Fig. 14(a) and (b) respectively.

Discussion

By using surface-adsorbed monodisperse nanospheres as a template, we have formed various hemispherical metal nanoparticles. The method is quite versatile with respect to the choice of metal. Nanoparticles with practically any thickness that can be produced; here we have demonstrated the range of optical properties, *i.e.*, absorbance that can be achieved. With gold, we can tune the peak position in the range from lower 500 to upper 800 nm. The size dependence we had explored in our earlier work was not exploited in the current work,[27] and that would significantly increase the extent of flexibility.

Gold nanoparticles have always been a very popular topic. Beside spheres, a wide variety of shapes such as shell, rod, disc, star *etc.*, can now be prepared. Some of common characteristics of gold nanoparticles can be cited; (1) The size under 100 nm is desirable for resonance of free electrons because larger sizes lead to excitation of higher-order modes other than the fundamental mode and lead to spectral broadening.[22,57] (2) Elongated shapes can support multiple resonance modes in

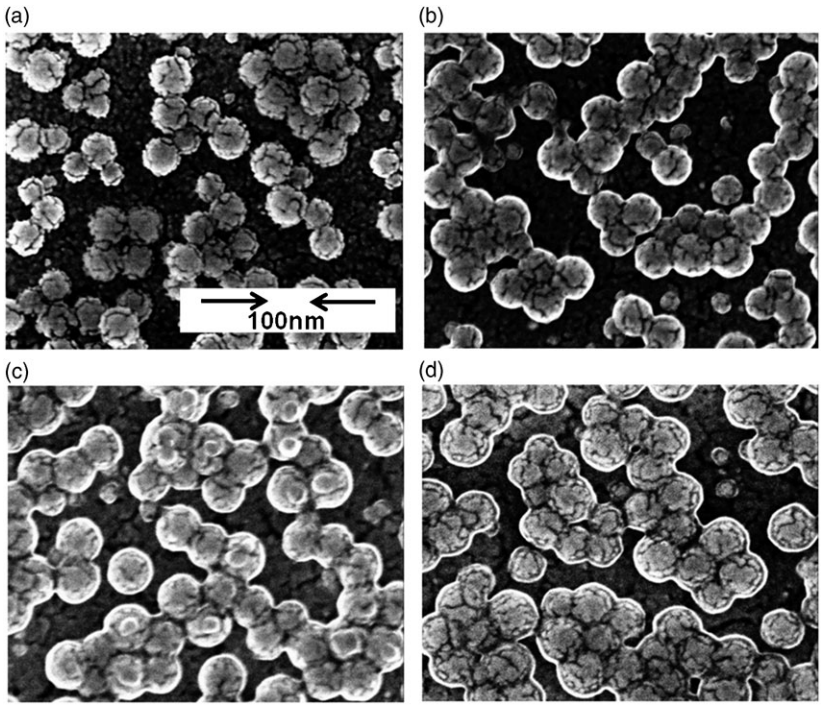

Fig. 11 SEM micrographs of the samples whose spectra are shown in Fig. 10. With longer reaction times, the thickening layer of the reaction product is seen on the gold particle surface. The maximum deposition thickness is not much more than 10 nm.

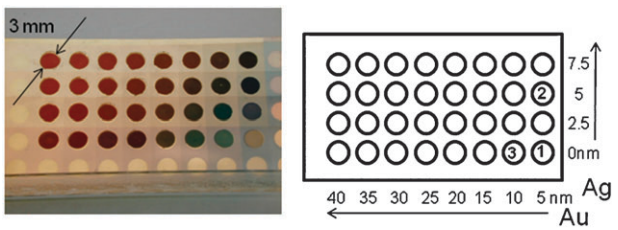

Fig. 12 A combinatorial approach for making composite nanoparticles. When a metal is deposited onto the nanosphere monolayer, a mechanical shutter masking the substrate is moved in a step-wise fashion. The resulting sample consists of particles with different deposition thicknesses. After the first deposition, the relative direction of the shutter movement is rotated 90° by rotating the sample. Then, in a fashion identical to the first deposition, the second metal is evaporated as the shutter is moved in a step-wise fashion. The final sample consists of metal particles with varying compositions. In the horizontal direction, the deposition thickness of gold was varied from 5 to 40 nm with an increment of 5 nm from right to left. Along the vertical direction, the silver deposition thickness was varied from 0 to 7.5 nm with an increment of 2.5 nm. The bottom row is without any adsorbed particle.

mutually perpendicular directions.[58,59] (3) Particularly strong near-field is generated at pointed ends. For a group of particles in close vicinity, the gap region between two neighboring particles is well-suited for generation of an intense "hot spot" desirable for a number of surface enhanced spectroscopic techniques.[9,12,60–62]

In view of this, our particle system is likely to pose a number of intriguing questions. Nanoparticles are densely packed so that there should be quite a few "hot spots" present. There have been reports that nano shells are more suited than solid spheres for generation of "hot spots",[9] and hemispherical metal nanoparticles are expected to have a similar advantage. Moreover, with the current system, the resonance effect of an individual particle can possibly be coupled to an optical nano-cavity formed by the top and bottom gold layers.

Silver and copper nanoparticles have been less extensively studied as gold nanoparticles because of difficulties of making and stabilizing them for investigation and applications.[59,63–65] We have demonstrated earlier the power of the current technique for application to surface-enhanced

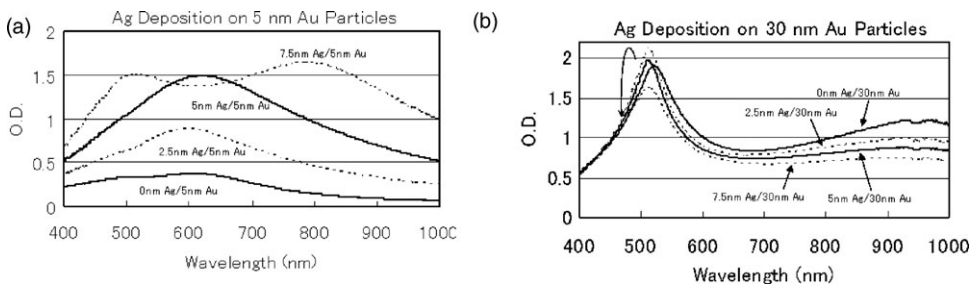

Fig. 13 Spectra of most spots for the combinatorial particle array shown in Fig. 12 With thinner gold deposition thicknesses, even a very thin silver deposition has a large effect in the resulting spectrum (see also Fig. S2 of the ESI†).

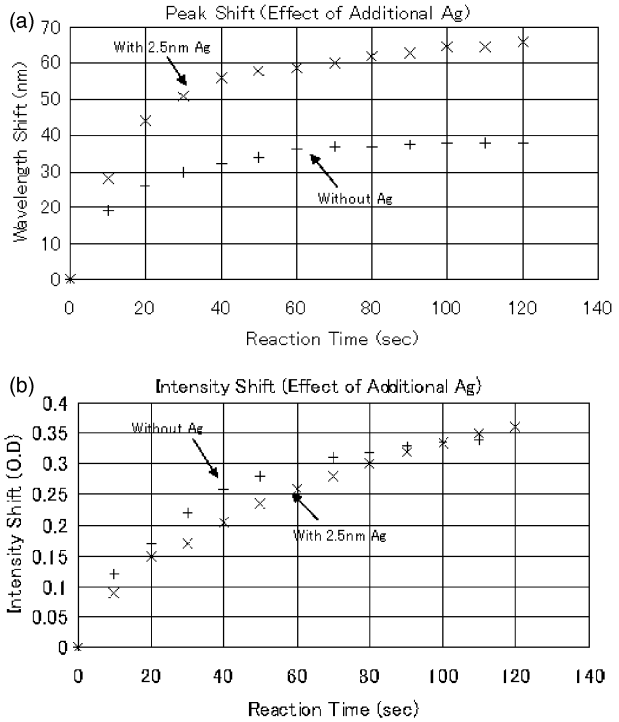

Fig. 14 Peak wavelength and intensity changes accompanying the ALP reaction for multi-layered metal nanoparticles.

fluorescence.[46,47] We were able to show that 50 fold enhancements were possible with hemispherical silver nanoparticles. Due to the uniformity of our silver particles, we could produce quantitative data, to our knowledge, for the first time which is a crucial requirement for clinical diagnostic applications. This was demonstrated by the excellent linearity with sandwich assays. The stability remains a hurdle, but we could confirm that the enhancement effect was quite strong after one month storage at ambient temperature, vanishing completely after some three months.

As important as the enhancement effect and stability might be, the ease of preparation and uniformity are crucial issues. Photos in Fig. 3 amply show that these particle surfaces can be produced in a meaningfully large area and the quality is rather uniform. From a practical point of view, uniformity is a great issue.[66]

The dependence of the peak position as well as the intensity on the refractive index of the environment has been long known and explored. Our earlier paper suggested the use of hemispherical gold nanoparticles for non-labeled biosensing in the late 90s,[48] and since then a number of groups beside our own have demonstrated the capability.[26,27,67] While disperse isolated gold nanoparticles possess an absorption peak that depend relatively in a straightforward manner on the surrounding refractive index, the current hemispherical nanoparticle exhibits a slightly more complex dependence. Depending on the incidence angle and polarization, the peak can be red- or blue-shifted upon adsorption of a thiol molecule.[68] In this work also, Fig. 4(c) gives a glimpse of the behavior of a shift or shoulder upon change in the refractive index. In future work, we plan to carry out a systematic study with gold deposition thicknesses around 15 nm spanning the range of 10 to 20 nm. Difference spectra before and after the ALP reaction are shown in Fig. 5. The particles formed by 10 nm deposition show an overall increase across the wavelength region measured here, but with the additional 5 nm thick gold, the total of 15 nm, the difference spectrum now shows a large negative peak. With thicker gold depositions, the change is still negative overall, but there is no longer any peak. At shorter wavelengths, the change is positive overall.

Fig. 6 show the enzyme reaction sequence. The absorbance below 450 nm is due to the NBT/BCIP solution so that it appears immediately upon injection of the substrate solution. In the control experiment, the change is detectable, but in comparison to the difference spectra in Fig. 5, it is insignificant; in those spectra in Fig. 4, the O.D. change in this wavelength regime is not noticeable. For further comparison, we performed enzyme reactions with a fewer number of ALP molecules. By diluting the ALP solution before physisorption, we explored the sensitivity limit. Fig. 7 show difference spectra for control experiments with various ALP dilution ratios. With 5000 fold dilution, the change becomes quite suppressed. On the other hand, when one carries out the same 5000 fold dilution experiment on 15 nm thick gold nanoparticles, we can clearly see change in the spectrum; if O.D. change is used an as indicator, it is as large as 0.3 around 750 nm. The colored product of the ALP-NBT/BCIP would make an interesting study on possible resonance effect between the substrate; we plan to carry out similar experiments with colorless product for a comparative study.

For colorimetric diagnostics, it is of advantage if the color change occurs in the wavelength regime where the human eye has a strong discriminatory power. Photos in Fig. 9 reveal that the color change is mostly from brown to blue. For spectroscopic comparison, the 15 nm gold particles exhibit the most striking difference spectrum, but for visual inspection, thicker gold depositions may be of greater utility.

The correlation between the product deposition thickness and spectral shift is important. Spectra and SEM micrographs were obtained from the same set of samples. They are shown in Fig. 10 and 11 respectively. While accurate assessment of the deposition thickness is not possible, these figures can, nonetheless, give an upper limit. With the 5 min reaction, the product, looking like a shell, is estimated to be 10 nm thick If it can be assumed that the shell growth at the initial stage of the enzyme reaction is linear, then the deposition thickness after 1 min must be approximately 2 nm or so. Such thin deposition leads to a significant spectral shift as can be seen in Fig. 10.

Finally we discuss the potential of a combinatorial approach for formation of metal nanoparticles. The photo in Fig. 12 shows an array of Ag/Au multilayer particles. The bottom row consists of spots of pure gold particles, with thicknesses ranging from 5 to 40 nm from right to left. Within each column, incrementally thicker silver is evaporated from bottom to top, corresponding to 2.5, 5 and 7.5 nm. Combinatorial chemistry was one time widely explored, but to our knowledge, this is one of the few reports on use of a combinatorial approach in metal nanoparticle formation. The photo shows that particles with 5 nm silver and 5 nm gold deposition are significantly more absorbing than the 10 nm

gold particles. Spectra of these spots are shown in Fig. 13, and comparison of the spectrum of the 5nmAg/5nmAu particles in Fig. 13(a) and that of 10 nm gold nanoparticle in Fig. 2(a) reveals a significant difference in the absorbing strength in the 620–650 nm region. Overall, deposition of silver on top of gold nanoparticles has effects somewhat similar to additional deposition of gold, but silver is more effective in altering the original spectrum, requiring less additional depositions.

To investigate whether multiple-layer metal nanoparticles behave differently in combination with the ALP reaction from single layer particles, we have started a preliminary investigation. In Fig. S1 (see the ESI†), the spots from the second column from right in Fig. 12 were used for the ALP reaction. While Fig. S1(c), data from particles consisting of 5 nm silver on top of 10 nm gold shows that the spectrum looks quite like that of 15 nm gold, the change accompanying the enzyme reaction is quite diminished. On the other hand, Fig. S1(b) shows that the additional 2.5 nm silver has a positive effect over the original 10 nm gold particles. The peak wavelength and peak intensity are plotted for these two types of particles in Fig. 14(a) and (b). While there is little improvement in the intensity change, the peak wavelength change is now almost twice as large.

This is just a preliminary result of the combinatorial approach to metal nanoparticle preparation. In this study we have limited ourselves to just gold and silver, and the incremental change was relatively large; in view of the fact, that a few nm change in the deposition thickness can make a significant difference as shown in connection with Fig. 5, a study using finer incremental changes is called for. The number of layers does not need to be limited to two, and any combination of deposition thicknesses and metals, in a variety of sequence is possible. Tunability is an important property.[13,67,69–73]

The application to the colorimetric enzyme reaction is only one small one. As we have demonstrated in the past, hemispherical metal nanoparticles can be successfully applied to other spectroscopic techniques such as surface-enhanced fluorescence spectroscopy and localized surface plasmon resonance (LSPR) sensing for non-labeled biomolecule detection. It is foreseen that these technique can benefit from the current combinatorial approach in the near future.

Conclusions

In this paper, we presented a simple scheme for preparing surface-adsorbed metal nanoparticles. The current technique is characterized by the flexibility of the type of metal that can be used for preparation of particles of an arbitrary size, thickness, and composition.

Using this technique, we prepared gold, silver and copper particles. The first two noble metals are of particular interest in the field of optics due to resonance of free electrons corresponding to the UV to visible regime. The resonance frequency is sensitively dependent on the refractive index of the surrounding media, and it promises to become a powerful tool for *in situ* investigation behavior of biological systems in close contact with noble metal nanoparticles. Gold has been the metal of choice for such applications, predominantly due to its stability. We investigated the dependence of the absorption peak on the deposited reaction of an enzyme reaction. This serves two purposes; in one sense, this can clearly demonstrate the near-field nature of the peak position. We can observe the extent of the near-field. By varying the reaction time, we formed insoluble layers of varying thickness. Another objective is to see if sensitivity of colorimetric enzyme assays can be improved. Using a plane gold surface as the control, we demonstrated that the detection threshold of the enzyme reaction can be reduced.

References

1 Y. Teramura, Y. Arima and H. Iwata, *Anal. Biochem.*, 2006, **357**, 208.
2 L. K. Kricka, *Clin. Chem.*, 1994, **40**, 347.
3 P. Fortina, L. J. Kricka, D. J. Graves, J. Park, T. Hyslop, F. Tam, N. Halas, S. Surrey and S. A. Waldman, *Trends Biotechnol.*, 2007, **25**, 145.
4 F. Yu, F. B. Persson, S. Lofas and W. Knoll, *Anal. Chem.*, 2004, **76**, 6765.
5 E. G. Matveeva, Z. Gryczynski and J. R. Lakowicz, *J. Immunol. Methods*, 2005, **302**, 26.
6 A. J. Haes, S. Zou, G. C. Schatz and R. P. Van Duyne, *J. Phys. Chem. B*, 2004, **108**, 109.
7 J.-S. Lee, A. K. R. Lytton-Jean, S. J. Hurst and C. A. Mirkin, *Nano Lett.*, 2007, **7**, 2112.
8 N. Félidj, J. Aubard, G. Lévi, J. R. Krenn, M. Salerno, G. Schider, B. Lamprecht, A. Leitner and F. R. Aussenegg, *Phys. Rev. B: Condens. Matter Mater. Phys.*, 2002, **65**, 075419.
9 C. E. Talley, J. B. Jackson, C. Oubre, N. K. Grady, C. W. Hollars, S. M. Lane, T. R. Huser, P. Nordlander and N. J. Halas, *Nano Lett.*, 2005, **5**, 1569.
10 J. C. Hulteen and R. P. Van Duyne, *J. Vac. Sci. Technol., A*, 1995, **13**, 1553.
11 L. Baia, M. Baia, J. Popp and S. Astilean, *J. Phys. Chem. B*, 2006, **110**, 23982.
12 L. Gunnarsson, T. Rindzevicius, J. Prikulis, B. Kasemo, M. Käll, S. Zou and G. C. Schatz, *J. Phys. Chem. B*, 2005, **109**, 1079.
13 N. J. Halas, *Proc. Natl. Acad. Sci. U. S. A.*, 2009, **106**, 3643.
14 T. A. Taton, C. A. Mirkin and R. L. Letsinger, *Science*, 2000, **289**, 1757.
15 P. Sevilla, F. Garcia-Blanco, J. V. Garcia-Ramos and S. Sanchez-Cortes, *Phys. Chem. Chem. Phys.*, 2009, **11**, 8342.
16 S. Diegoli, P. M. Mendes and J. A. Preece, in *Nanomeeting 2007 International Conference*, Reviews and Short Notes, 2007, pp. 277.
17 J. S. Ahn, P. T. Hammond, M. F. Rubner and I. Lee, *Colloids Surf., A*, 2005, **259**, 45.
18 R. Dahint, E. Trileva, H. Acunman, U. Konrad, M. Zimmer, V. Stadler and M. Himmelhaus, *Biosens. Bioelectron.*, 2007, **22**, 3174.
19 C. R. Yonzon, D. A. Stuart, X. Zhang, A. D. McFarland, C. L. Haynes and R. P. Van Duyne, *Talanta*, 2005, **67**, 438.
20 F. Le, D. W. Brandl, Y. A. Urzhumov, H. Wang, J. Kundu, N. J. Halas, J. Aizpurua and P. Nordlander, *ACS Nano*, 2008, **2**, 707.
21 A. B. R. Mayer, W. Grebner and R. Wannemacher, *J. Phys. Chem. B*, 2000, **104**, 7278.
22 U. Kreibig and M. Vollmer, *Optical Properties of Metal Clusters*, Springer, Heidelberg, 1995.
23 A. D. Ormonde, E. C. M. Hicks, J. Castillo and R. P. Van Duyne, *Langmuir*, 2004, **20**, 6927.
24 C. R. Yonzon, E. Jeoung, S. Zou, G. C. Schatz, M. Mrksich and R. P. Van Duyne, *J. Am. Chem. Soc.*, 2004, **126**, 12669.
25 T. Vo-Dinh, M. Y. K. Hiromoto, G. M. Begun and R. L. Moody, *Anal. Chem.*, 1984, **56**, 1667.
26 M. Himmelhaus and H. Takei, *Sens. Actuators, B*, 2000, **63**, 24.
27 H. Takei and M. Himmelhaus, in *Progress in Nano-Electro-Optics III*, Springer, Berlin, 2005.
28 S. J. Oldenburg, G. D. Hale, J. B. Jackson and N. J. Halas, *Appl. Phys. Lett.*, 1999, **75**, 1063.
29 X. Sun and M. Hagner, *Langmuir*, 2007, **23**, 9147.

30 W. Rechberger, A. Hohenau, A. Leitner, J. R. Krenn, B. Lamprecht and F. A. Aussenegg, *Opt. Commun.*, 2003, **220**, 137.
31 H. Wang, D. W. Brandl, F. Le, P. Nordlander and N. J. Halas, *Nano Lett.*, 2006, **6**, 827.
32 R. G. Freeman, K. C. Grabar, K. J. Allison, R. M. Bright, J. A. Davis, A. P. Guthrie, M. B. Hommer, M. A. Jackson, P. C. Smith, D. G. Walter and M. J. Natan, *Science*, 1995, **267**, 1629.
33 K. Kneipp, Y. Wang, H. Kneipp, L. T. Perelman, I. Itzkan, R. R. Dasari and M. S. Feld, *Phys. Rev. Lett.*, 1997, **78**, 1667.
34 H. Wang, G. P. Goodrich, F. Tam, C. Oubre, P. Nordlander and N. J. Halas, *J. Phys. Chem. B*, 2005, **109**, 11083.
35 N. P. W. Pieczonka and R. F. Aroca, *ChemPhysChem*, 2005, **6**, 2473.
36 G. Chumanov, K. Sokolov, B. M. Gregory and T. M. Cotton, *J. Phys. Chem.*, 1995, **99**, 9466.
37 M. Osawa, *Top. Appl. Phys.*, 2001, **81**, 163.
38 M. Osawa, K. Ataka, K. Yoshii and Y. Nishikawa, *Appl. Spectrosc.*, 1993, **47**, 1497.
39 S. Lal, N. K. Grady, J. Kundu, C. S. Levin, J. B. Lassiter and N. J. Halas, *Chem. Soc. Rev.*, 2008, **37**, 898.
40 J. R. Lakowicz, C. D. Geddes, I. Gryczynski, J. Malicka, Z. Gryczynski, K. Aslan, J. Lukomska, E. Matveeva, J. Zhang, R. Dadugu and J. Huang, *J. Fluoresc.*, 2004, **14**, 425.
41 K. Aslan, Z. Leonenko, J. R. Lakowicz and C. D. Geddes, *J. Fluoresc.*, 2005, **15**, 643.
42 F. Xie, M. S. Baker and E. M. Goldys, *J. Phys. Chem. B*, 2006, **110**, 23085.
43 J. Kümmerlen, A. Leitner, H. Brunner, F. R. Aussenegg and A. Wokaun, *Mol. Phys.*, 1993, **80**, 1031.
44 S. Nie and S. R. Emory, *Science*, 1997, **275**, 1102.
45 X. Zhang, M. A. Young, O. Lyandres and R. P. Van Duyne, *J. Am. Chem. Soc.*, 2005, **127**, 4484.
46 T. Yamaguchi, T. Kaya and H. Takei, *Anal. Biochem.*, 2007, **364**, 171.
47 T. Yamaguchi, T. Kaya, M. Aoyama and H. Takei, *Analyst*, 2009, **134**, 776.
48 H. Takei, *J. Vac. Sci. Technol., B*, 1999, **17**, 1906.
49 H. Takei and N. Shimizu, *Langmuir*, 1997, **13**, 1865.
50 S. Link and M. A. El-Sayed, *J. Phys. Chem. B*, 1999, **103**, 8410.
51 Z.-H. Lin and H.-T. Chang, *Langmuir*, 2008, **24**, 365.
52 N. Toshima and T. Yonezawa, *New J. Chem.*, 1998, **22**, 1179.
53 X. Zhang, M. Tsuji, S. Lim, N. Miyamae, M. Nishio, S. Hikino and M. Umeza, *Langmuir*, 2007, **23**, 6372.
54 X.-D. Xiang, X. Sun, G. Briceno, Y. Lou, K.-A. Wang, H. Chang, W. G. Wallace-Freedman, S.-W. Chen and P. G. Schultz, *Science*, 1995, **268**, 1738.
55 M. Himmelhaus and H. Takei, *Phys. Chem. Chem. Phys.*, 2002, **4**, 496.
56 T. Endo, K. Kerman, N. Nagatani, H. M. Hiepa, D.-K. Kim, Y. Yonezawa, K. Nakano and E. Tamiya, *Anal. Chem.*, 2006, **78**, 6465.
57 K. L. Kelly, E. Coronado, L. L. Zhao and G. C. Schatz, *J. Phys. Chem. B*, 2003, **107**, 668.
58 C. L. Haynes, A. D. McFarland, L. L. Zhao, R. P. Van Duyne, G. C. Schatz, L. Gunnarson, J. Prikulis, B. Kasemo and M. Käll, *J. Phys. Chem. B*, 2003, **107**, 7337.
59 M. W. Knight and N. J. Halas, *New J. Phys.*, 2008, **10**, 105006.
60 H. Wang, C. S. Levin and N. J. Halas, *J. Am. Chem. Soc.*, 2005, **127**, 14992.
61 K. Sokolov, G. Chumanov and T. M. Cotton, *SPIE*, 1995, **2547**, 117.
62 K. Sokolov, G. Chumanov and T. M. Cotton, *Anal. Chem.*, 1998, **70**, 3898.
63 D. Mott, J. Galkowski, L. Wang, J. Luo and C.-J. Zhong, *Langmuir*, 2007, **23**, 5740.
64 H. Wang, F. Tam, N. K. Grady and N. J. Halas, *J. Phys. Chem. B*, 2005, **109**, 18218.
65 G. H. Chan, J. Zhao, E. M. Hicks, G. C. Schatz and R. P. Van Duyne, *Nano Lett.*, 2007, **7**, 1947.
66 F. Ni and T. M. Cotton, *Anal. Chem.*, 1986, **58**, 3159.
67 H. M. Hiep, T. Endo, M. Saito, M. Chikae, D. K. Kim, S. Yamamura, Y. Takamura and E. Tamiya, *Anal. Chem.*, 2008, **80**, 1859.
68 H. Takei, M. Himmelhaus and T. Okamoto, *Opt. Lett.*, 2002, **27**, 342.
69 C. A. Foss, Jr., G. L. Horynak, J. A. Stockert and C. R. Martin, *J. Phys. Chem.*, 1994, **98**, 2963.
70 T. R. Jensen, M. D. Malinsky, C. L. Haynes and R. P. Van Duyne, *J. Phys. Chem. B*, 2000, **104**, 10549.
71 A. M. Alak and T. Vo-Dinh, *Anal. Chem.*, 1989, **61**, 656.
72 K. S. Lee and M. A. El-Sayed, *J. Phys. Chem. B*, 2006, **110**, 19220.
73 C. L. Haynes and R. P. Van Duyne, *J. Phys. Chem. B*, 2001, **105**, 5599.

